

Article

X-ray Computed Tomography (CT) Scanning Is a Non-Destructive and Modern Technique to Identify and Assess the Characteristics of *Armillaria solidipes* Pathogen Infections in Poplar Roots

Ping Zhang ^{1,2}, Mingru Kong ¹, Guangqiang Xie ¹, Theo van der Lee ², Lihai Wang ^{1,*} and Yanqiu Xing ^{1,*}

¹ Heilongjiang Provincial Key Laboratory of Forest Sustainable Management and Environmental Microbial Engineering, Northeast Forestry University, Harbin 150040, China

² Biointeractions and Plant Health, Wageningen University & Research, 6700 AA Wageningen, The Netherlands

* Correspondence: wanglihai60@yeah.net (L.W.); yanqiuqing@nefu.edu.cn (Y.X.)

Abstract: (1) Objective: The opacity of soils complicates studies of root infection. An example of this is the infection of *Armillaria solidipes* on poplar (*Populus davidiana* × *Populus alba* var. *pyramidalis* Louche) roots systems, which risks damaging trees. (2) Methods: Only one of the four tested substrates for tree species was shown to be suitable to perform X-ray computed tomography (CT). Three-dimensional (3D) imaging was used to reconstruct the root system of poplar seedlings and the changes caused by the infection. (3) Results: We developed a protocol to efficiently grow poplar on a synthetic matrix, vermiculite, that allows for monitoring the root system by X-ray CT. Poplar 3D reconstruction of the root system was automated using the software Win-RHIZO, and various infection parameters were identified. (4) Conclusions: Our procedure allows for monitoring the infection of root systems and provides new opportunities to characterize the complex *Armillaria solidipes* poplar interaction using X-ray CT.

Keywords: *Populus davidiana* × *P. alba* var. *pyramidalis* Louche; X-ray computed tomography (CT); *Armillaria solidipes*; root etiology; 3D reconstruction; forests disease



Citation: Zhang, P.; Kong, M.; Xie, G.; van der Lee, T.; Wang, L.; Xing, Y. X-ray Computed Tomography (CT) Scanning Is a Non-Destructive and Modern Technique to Identify and Assess the Characteristics of *Armillaria solidipes* Pathogen Infections in Poplar Roots. *Forests* **2022**, *13*, 1963. <https://doi.org/10.3390/f13111963>

Academic Editor: Simon Francis Shamoun

Received: 14 October 2022

Accepted: 18 November 2022

Published: 21 November 2022

Publisher's Note: MDPI stays neutral with regard to jurisdictional claims in published maps and institutional affiliations.



Copyright: © 2022 by the authors. Licensee MDPI, Basel, Switzerland. This article is an open access article distributed under the terms and conditions of the Creative Commons Attribution (CC BY) license (<https://creativecommons.org/licenses/by/4.0/>).

1. Introduction

Globally, *Armillaria* root rot (ARR) is a well-known infectious disease that causes economic losses to forestry in more than 70 countries, including China, the United States, the United Kingdom, France, Canada, and Australia [1]. The primary pathogens that cause *Armillaria* root rot are the Basidiomycota fungi, such as *Armillaria mellea* and *Armillaria solidipes*, which harm up to 500 species of host trees [2]. *A. solidipes* has also been described in some studies as *Armillaria ostoyae* (Romagnesi) Herink, the most important pathogen of conifers in Europe [3,4]. In addition to infecting trees, these two species of *Armillaria* also infect some shrubs. ARR mainly infects the root systems of trees. In the early stages of infection, the symptoms are not observable, and the crown's appearance does not change. In the late stages of disease, the root neck and root cortex rot, and a white fan-shaped biofilm develops between the cortex and the xylem. The xylem becomes white, spongy, and decays, making the wood useless [5]. In addition, dark brown or black Rhizomorph cords appear on the surface, cortex, and nearby soil. More than 50 species of *Armillaria* pathogenic fungi have been reported globally, among which *A. mellea* and *A. solidipes* are the most common species. Coetzee et al. [6] found that in 2021, *Armillaria* spp infested grape plantations in California, USA, causing a 10%–40% reduction in annual grape yields. Moreover, *A. solidipes* infections killed native conifers in South America and Europe, resulting in more than 30% economic losses [7].

For years, etiological studies of tree root rot have been difficult because physical methods for excavating the root system and visual observations of the infected root system are

used to assess disease incidence and index [8]. This sampling method causes damage to the plant root system [9]. In addition, physical excavation often cannot obtain a complete root system structure and monitor the degree of disease occurrence in real-time [9]. As a result, several nondestructive testing techniques have been developed. For example, Han et al. [10] successfully used medical X-ray computed tomography (X-ray CT) technology to separate the roots of potatoes (*Solanum tuberosum*). They confirmed that the root system of diseased potato is simple, and *Streptomyces scabies* infection affects the growth of underground tuberous roots of potato. The study by Han et al. [11] was the first to apply X-ray CT technology in plant pathology research. They later used X-ray CT to inoculate the pathogenic *S. scabies* into the soil for planting potatoes. They found that there was more rotting of seed tubers, relative to other tubers [11]. Peters et al. [12] measured the embolism of woody roots and stems caused by drought in *Acacia aneura*, *Cedrus deodara*, *Eucalyptus crebra*, *Eucalyptus saligna*, and *Quercus palustris*. The X-ray CT visualization was used to visualize the accumulation of the xylem embolism in the stems and roots of intact plants that were naturally dehydrated to varying levels of water stress. Chigwaya et al. [13] used the X-ray CT system to detect internal browning (IB) in “Fuji” apple (*Malus × domestica* Borkh) by determining the changes in CO₂ concentrations. High-resolution scans showed that due to membrane damage and flooding of the intercellular spaces with cytosol, fruit tissues with IB had a lower total porosity and pore connectivity than the unaffected fruit tissues.

Improvement in the sensitivity of the ray detector and shortening of the acquisition time in the X-ray CT system have made it easier to repeatedly scan the same sample. As a result, the configuration of plant roots in the soil can be observed in real-time. X-ray CT technology has been used in clinical medical testing for more than 30 years. It is used in several experiments that involve observing human internal lesions and fine structures in the body, such as cerebral blood vessels and small bronchioles in the lungs, as well as intrahepatic bile ducts [14,15]. Therefore, we propose the use of X-ray CT imaging in studies of diseased plant roots. However, in nature, the soil medium and plant root densities vary, and they are indistinguishable in X-ray CT imaging [16,17]. Therefore, the soil is one of the interference factors affecting X-ray CT imaging.

This study aimed to do the following: (i) Design a substrate that can support the growth of poplar and be suitable for X-ray CT imaging. (ii) Generate both internal and 3D reconstructions of the root system. (iii) Establish procedures to effectively analyze infection parameters and automate the analysis of poplar. (iv) Exploiting the methods to investigate poplar–*A. solidipes* interactions during infection.

2. Materials and Methods

2.1. Materials

A. solidipes (numbered A2001) rhizomorphs from infected poplar wood were used as the pure cultures. A2001 strain internal transcribed spacer information was stored in National Center for Biotechnology Information (NCBI) GenBank, with the accession number OP787670.1. The *A. solidipes* strain was preserved in the Heilongjiang Provincial Sustainable Forest Management and Environmental Microbial Engineering Laboratory at the Northeast Forestry University.

The *P. davidiana* × *P. alba* var. *pyramidalis* Louche cultivar, which is highly susceptible to *A. solidipes*, was used in investigations. Seedlings were grown through stem differentiation, transferred to the rooting medium, and grown for four weeks. Healthy tissue culture seedlings with the same leaf length, width, and plant height were selected for transplantation.

2.2. Preparation and Design of Experimental Samples

Rooted poplar seedlings were transplanted into the non-woven pot, diameter × height × bottom diameter (26 × 35 × 18) cm, with sand + 1/2-strength Murashige and Skoog’s macronutrient (MS), clay + 1/2 MS, loam + 1/2 MS, and vermiculite + 1/2 MS. The size of the seedling pots was 26 × 35 × 18 cm. After transferring the seedlings, 50 mL 1/2 MS culture

solution was added to each pot and thoroughly mixed to ensure uniform distribution of various nutrient solutions in the soil. Seedlings were grown in a greenhouse with a temperature of 25 °C and a daily light of 16 h. In addition, 50 mL of water was added to the pots every ten days. Healthy seedlings with a growth cycle of 70 days and no disease symptoms were selected for the experiments. The greenhouse location was located at Harbin (126.60° E, 45.70° N), Heilongjiang Province, China. The treatment and control groups were replicated three times, with 12 seedlings per replicate.

2.3. Determination of the Growth Index of Poplar

To verify the effects of each soil matrix on poplar growth, the leaf width, leaf length, lateral root length, lateral root number, taproot root length, and plant height were measured. The plant height, leaf length and width, and other indicators were measured and recorded using vernier calipers (SATA91511, Shanghai, China).

2.4. Poplar Root Infection by *A. solidipes*

To infect the poplar roots, *A. solidipes* spores were cultured on a PDA plate media at 26 °C for 15 days, and were inoculated into a new PD fluid medium at 160 rpm for 10~15 d. Poplar roots were infected when the spore *OD600* concentration reached 1.8×10^8 CFU/mL. The roots of the experimental group were inoculated with 50 mL of *A. solidipes* fermentation broth using a syringe. The control group was inoculated with the same volume of sterile water.

2.5. X-ray CT Analysis of Poplar Root

After infection of the poplar with *A. solidipes*, the plants were allowed to grow for 70 days. Then, five potted poplar seedlings with consistent growth were randomly selected from each experimental group for X-ray CT layer-by-layer scanning (NeuViz 128 CT, Neusoft Medical Virtual Tour, Shenyang, China). The scanning parameters were as follows: Helical, 120 kV, 90 ms exposure time, layer thickness 1 mm, layer spacing 1 mm, 8 layers/revolution, and helical pitch 5 mm/revolution. The preliminary study found that the CT dose index (CTDI) was 45.19 mGy, while the dose length product (DLP) was 731.9 mGy*cm. After scanning, a 128-bit tomographic sequence image with a resolution of 256 × 256 pixels per inch (PPI) was obtained. The volume data of the root system images of the poplar were imported into the Neusoft workstation. After proper filtering, interpolation, and encapsulation preprocessing, the image processing software Avizo Fire (V 9.0, ThermoFisher scientific, Waltham, MA, USA) was used for imaging. Processed images were evaluated for image quality by two X-ray CT radiologists and two plant root researchers. The image quality was divided into two levels, normal image development and abnormal image development. The image quality criteria applied in the normal display are as follows: (i) complete displays of the entire root system of the poplar, (ii) the minimum measurement diameter of the displayed roots is less than or equal to 1.5 mm, and (iii) root images can be observed in 3D reconstruction. Abnormal images cannot meet the above three requirements.

2.6. 3D Reconstruction of the Root System Architecture of the Poplar

The 3D volume rendering function of the RadiAnt DICOM Viewer (V 2020.2.3, Poznan, Poland) software was used for the 3D reconstruction of the root system on segmented images. Then, Image J 1.52p software was used to quantify the area of the internal decay in the roots of the poplar within the image. The specific operation steps were to extract the boundary, convert the image to 8-bit, select the appropriate threshold, and adjust to the edge demo image. Gaussian blur was used to fill in the discontinuous signals (if the boundaries were too large, they were manually filled), inverted to obtain the rot mask, fill the holes, and finally obtain the rot data. Last, the root system analysis software Win-RHIZO 2017a (Regent Instruments, Inc., Quebec, QC, Canada) was used to calculate the total root length and root forks, among others, using the findings from the manual measurements.

2.7. Statistical Methods and Analysis

The Origin 2021 (learning version, Northampton, MA, USA) software was used for the data analysis. Comparison of the means was performed by one-way analysis of variance followed by the Duncan's multiple range test for comparison of the means between the experimental and control groups. $p \leq 0.05$ was set as the threshold for statistical significance.

3. Results

3.1. Effects of Different Combinations of Soil Matrices on the Growth of Poplar

To investigate the effects of different combinations of soil culture medium on poplar growth, poplar seedlings that had been grown for 70 days were selected, and their growth indices were determined. Figure 1 shows that the differences between the four soil matrices with regards to the two indices of leaf length and width were insignificant ($p > 0.05$). There were significant differences in the lateral root length between poplar planted in the combined soil matrix of the vermiculite + 1/2 MS and those planted in the combined soil matrix of sand + 1/2 MS, clay + 1/2 MS, and loam + 1/2 MS ($p < 0.05$). The combination soil matrix of clay + 1/2 MS had the greatest effects on the lateral root length. Differences in the lateral root number of poplar between the soil matrix of sand + 1/2 MS, and the soil matrices of clay + 1/2 MS and loam + 1/2 MS were significant ($p < 0.05$). The clay + 1/2 MS combination soil matrix had the smallest lateral root number. There were significant differences in the main root length index between the poplar planted in soil combination matrices of vermiculite + 1/2 MS and clay + 1/2 MS ($p < 0.05$). Differences in plant height between the poplar planted in the soil matrix of vermiculite + 1/2 MS, sand + 1/2 MS, clay + 1/2 MS, and loam + 1/2 MS were significant ($p < 0.05$). In conclusion, using vermiculite + 1/2 MS as the combined soil matrix had minimal effects on the leaf width, leaf length, lateral root length, lateral root number, taproot root length, and plant height of the poplar. The clay + 1/2 MS had marked effects on the lateral root length, lateral root number, taproot root length, and plant height of the poplar.

3.2. Effects of Different Combinations of Soil Matrix on the Imaging Quality of X-ray CT

The scanning of poplar roots using the X-ray machine CT and after image software processing showed that poplar roots in the sand + 1/2 MS combination soil matrix had irregular changes in density, and no root structure could be identified (Figure 2A). The roots from the clay + 1/2 MS combination soil matrix showed irregular changes in density and were relatively concentrated; the complete root structures could not be visualized (Figure 2B). The soil matrix of the loam + 1/2 MS combination also exhibited irregular density changes, and local root development was visualized but not complete (Figure 2C). Figure 2D shows the vermiculite + 1/2 MS combination soil matrix with intact roots with the least background interference. In summary, the combination of the vermiculite and 1/2 MS soil matrix is suitable for X-ray CT detection of poplar roots.

3.3. Internal Decay of Poplar Roots after *A. solidipes* Infections

To obtain detailed and quantitative information about *A. solidipes* on the internal decay of poplar roots, X-ray CT was used to scan the roots layer by layer. Figure 3A shows the root system of the control group with complete main and lateral roots. The density of the epidermis is evenly distributed from the top to the bottom. Moreover, the root systems of poplar that had been infected by *A. solidipes* were largely intact, the main roots were visible, lateral roots disappeared, and density distributions of the epidermis from top to bottom were uneven (Figure 3C). Analysis of the inside of roots revealed that the roots of the control group had a regular epidermis from top to bottom and a uniform internal density (Figure 3B). In contrast, the root epidermis of poplar after infection by *A. solidipes* showed irregular shape changes from top to bottom, with uneven internal density changes (Figure 3D). After measuring the lesion area, it was found that the top-to-bottom root rot areas at the 2 cm and 3 cm positions were 0.11 mm and 0.1 mm higher than those

of the control group (Figure 4), respectively. These results show that *A. solidipes* has a high pathogenicity to the roots of poplar. Different disease expressions were observed at different locations, the root tip was upward for the internal decay of the epidermis, phloem, and xylem.

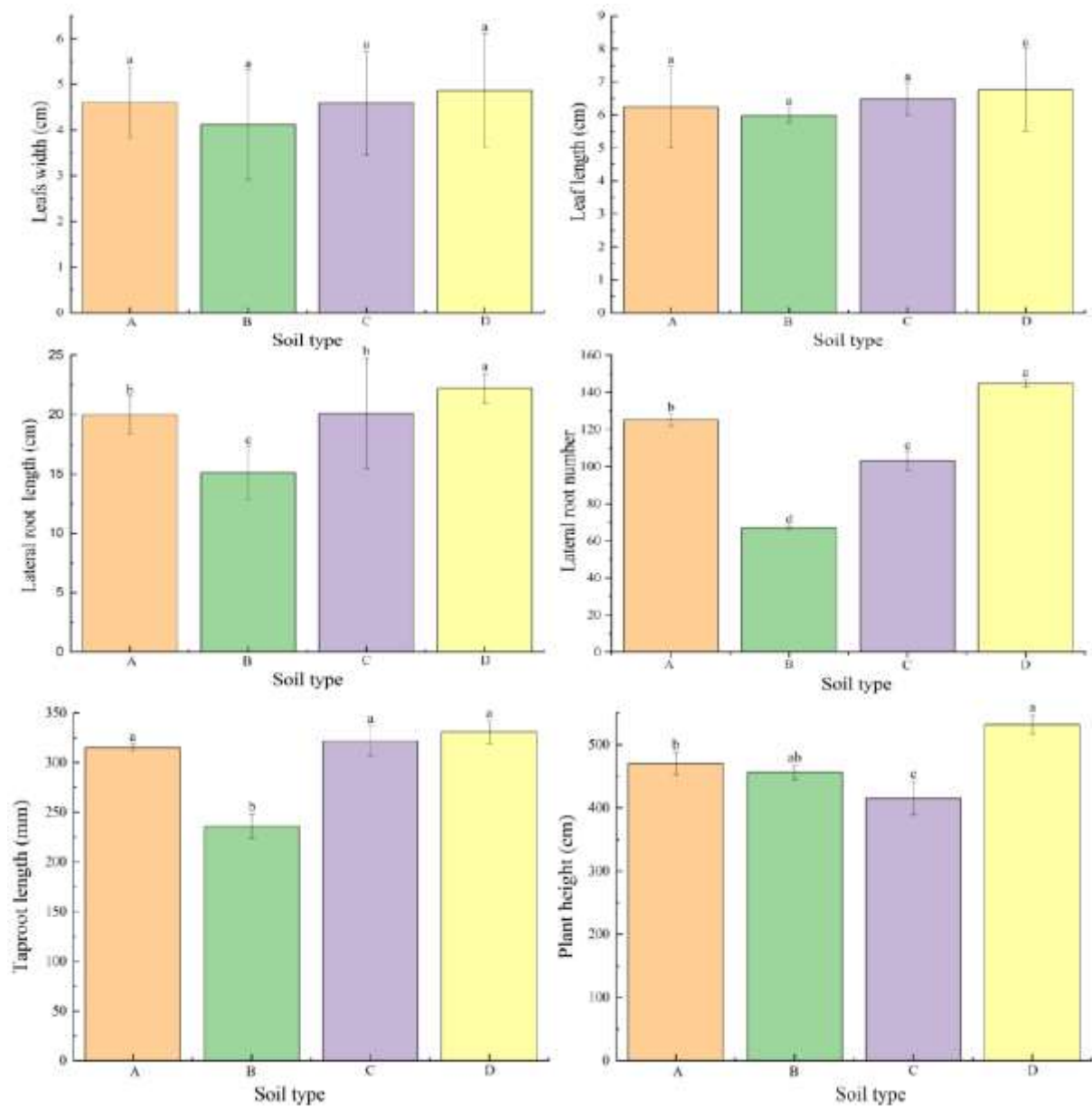


Figure 1. The effects of different media on the growth of poplar. A: sand + 1/2 MS; B: clay + 1/2 MS; C: loam + 1/2 MS; D: vermiculite + 1/2 MS. The graphical values denote the means for $n = 4$; the bar is four experimental averages; bars with different a, b, and c letters are significantly different (ANOVA, $p < 0.05$).

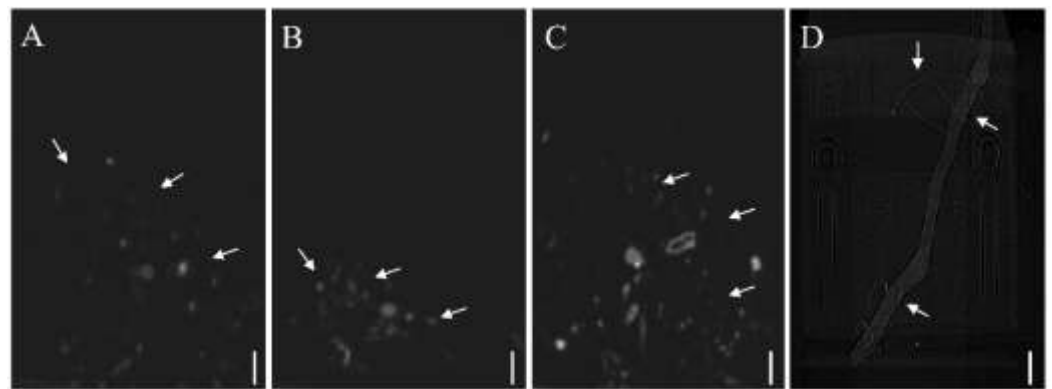


Figure 2. X-ray CT imaging of roots of poplar seedlings in different soil types. (A) Sand + 1/2 MS; (B) clay + 1/2 MS; (C) loam + 1/2 MS; (D) vermiculite + 1/2 MS. The scale is 1 cm. The white arrow represents the location of the X-ray CT imaging density.

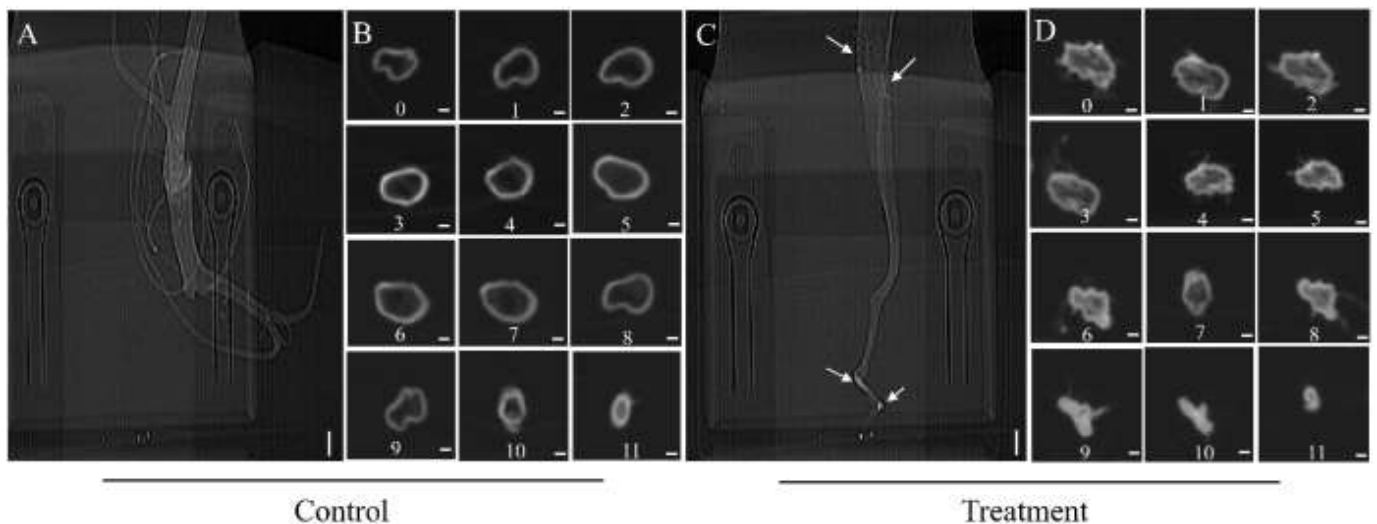


Figure 3. X-ray CT imaging of the root of poplar. (A) A preview of the root system; (B) different cross-sectional views of the root; (C) preview of the root system; (D) different cross-sections of the root system. The number represents the cross section (cm) of the root system from top to bottom. The scales (A,C) are 0.5 cm, while scales (B,D) are 0.2 mm. The white arrow represents the location of the density changes.

3.4. Effects of *A. solidipes* Infection on Root Architecture of Poplar

To study the effects of *A. solidipes* infection on the root architecture of poplar, a multi-view 3D reconstruction of root images using X-ray CT was performed. Figure 5(A1–F1) shows that the anterior, posterior, left, right, superior, and inferior faces of the root system of poplar were complete in the control group. The main and lateral roots are also shown. All parts of the poplar roots had the same color imaging, without observable density changes. Figure 5 shows that (A2–F2) the anterior, posterior, left, right, superior, and inferior faces of poplar roots in the treatment group were incomplete, while the main roots were thinner from top to bottom. In addition, poplar roots had inconsistent color imaging with observable internal density changes. The poplar in the treatment group had no lateral root (Figure 5(A2–D2)), and a solid black shadow was seen in the apical region (Figure 5(E2–F2)).

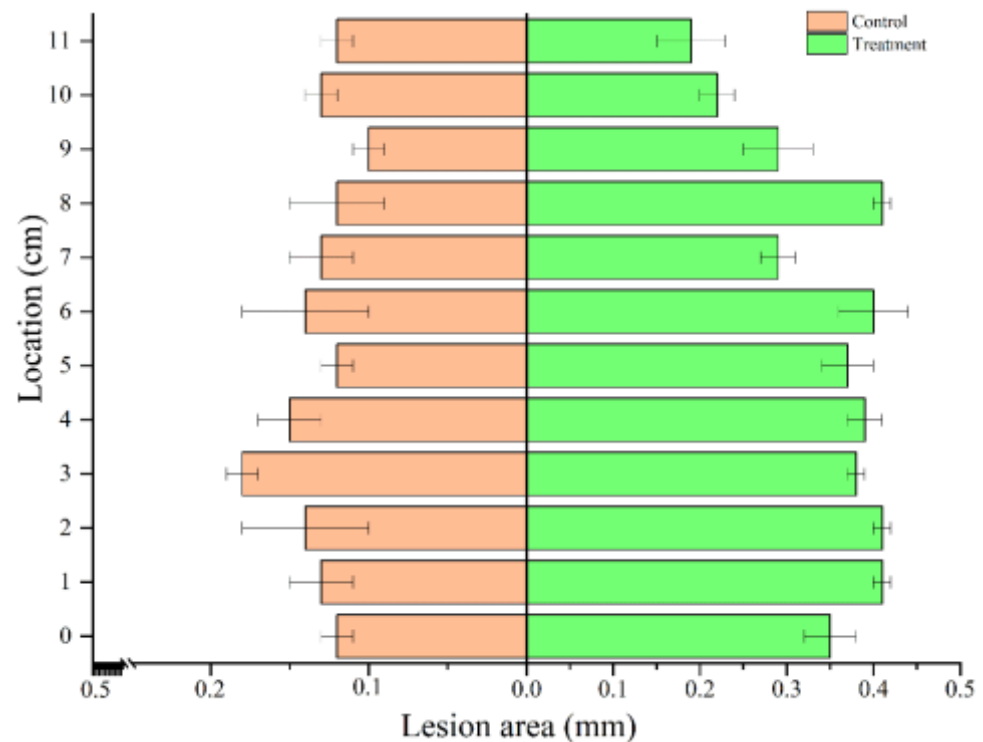


Figure 4. Diseased areas on cross-section roots of poplar. Values and errors are the averages of three trials, (one-way analysis of variance, ANOVA, $p < 0.05$).

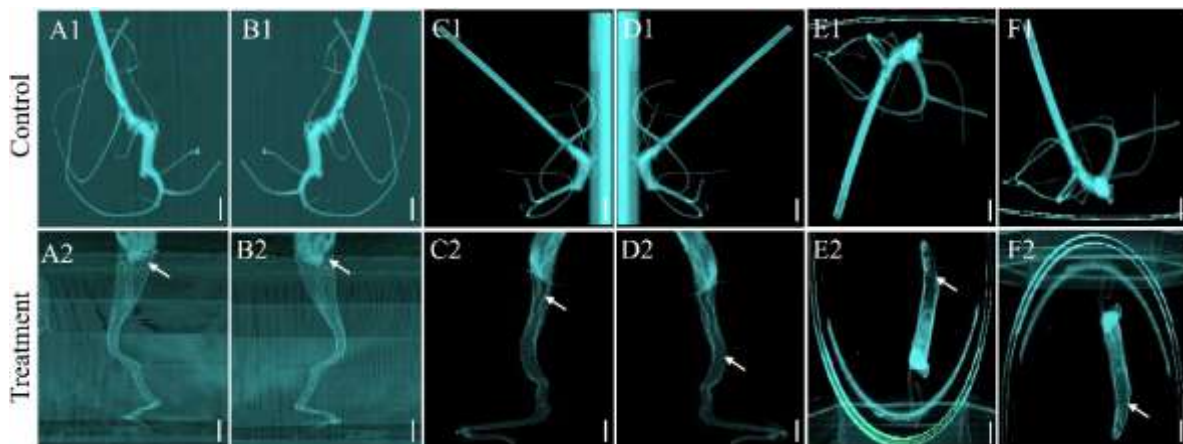


Figure 5. A 3D reconstruction of poplar roots from different perspectives. (A1,A2) anterior; (B1,B2) posterior; (C1,C2) left; (D1,D2) right; (E1,E2) superior; (F1,F2) inferior. The scale is 1 cm. The white arrow represents the locations of the density changes.

The 3D reconstruction of the root system index of the poplar was measured. Table 1 shows that the total root length of poplar in the treatment group was reduced by 128 cm, compared with the control group ($p < 0.05$). The total root volume of the poplar in the treatment group decreased by 0.36 cm^3 , relative to the control group ($p < 0.05$). The number of root tips for poplar in the treatment group decreased by 33, compared with the control group ($p < 0.05$). The root forks of poplar in the treatment group decreased by 2.81, compared with the control group ($p < 0.05$). Moreover, the total surface areas of the poplar roots in the treatment group decreased by 8.37 cm^2 , compared with the control group ($p < 0.05$). The root average diameters between the treatment and control groups were comparable ($p > 0.05$). These manual measurements were consistent with those obtained by

the Win-RHIZO 2017 software after the 3D reconstruction. Therefore, *A. solidipes* infection affected the root structure indices of the poplar.

Table 1. Root architecture indices of poplar.

Root Architecture Index	Manual		Soft	
	Control	Treatment	Control	Treatment
Total root length (cm)	273 ± 1.23 a	135 ± 1.34 b	260 ± 6.52 a	132 ± 9.23 b
Total root volume (cm ³)	0.83 ± 0.04 a	0.52 ± 0.04 b	0.87 ± 0.16 a	0.51 ± 0.18 b
Root forks	8.86 ± 0.12 a	5.45 ± 0.59 b	8.31 ± 1.45 a	5.50 ± 1.97 b
Number of root tip	85.56 ± 1.03 a	51.79 ± 1.43 b	84.00 ± 2.59 a	51.00 ± 4.11 b
Root average diameter (mm)	6.01 ± 0.87 a	5.31 ± 0.45 a	5.59 ± 1.59 a	5.38 ± 1.12 a
Root surface area (cm ²)	14.47 ± 0.67 a	7.34 ± 1.01 b	15.47 ± 1.59 a	7.10 ± 2.59 b

Results are shown as mean ± standard error (SE) for n = 3. Means followed by the same letter(s) within a column are not significantly different, as determined by Duncan's test ($p < 0.05$).

4. Discussion

The X-ray CT imaging technique was used to assess the ARR infection process of the poplar root. The excavation method is usually used to extract the diseased tissue, whereas the severity of disease is evaluated through visual observation, both of which reveal pathogenic infections in plant roots. However, this method requires high human operation [18], which results in many observation errors [19], root displacement, and breakage, as well as water loss. Wolfgang et al. [20] showed that in the study of the section wall, glass wall, and drilling method, although destructive sampling was not required, it was difficult to obtain complete and accurate 3D morphological data. In this study, the X-ray CT method was used to acquire complete images and 3D images of the root system, avoiding the above challenges. Van der Weele et al. [21] used a camera imaging system to image *Arabidopsis* and tomato seedlings growing in test tubes. They reported that this method is easier to operate and is less costly. However, it requires a high culture medium transparency, making it unsuitable to study the roots of woody plants. In this regard, we used the X-ray CT imaging technique to assess the ARR infection processes of the poplar root.

First, we studied the effects of different soil matrices on the imaging quality of X-ray CT. Under the vermiculite + 1/2 MS medium, images of the root system were good, showing less shading by the soil background. The root imaging quality was poor in the sand + 1/2 MS, clay + 1/2 MS, and loam + 1/2 MS soil matrices, which showed significant shading by the soil background. As the soil culture medium contained iron, copper, and other components, the density differences of the plant root system were similar or different, thus the plant root system could not be realistically displayed [22,23]. To overcome this challenge, we selected vermiculite + 1/2 MS as the culture medium, which has slight differences in density when compared with the poplar roots (± 230 HU) [24]. In this medium, the root system of the plant can be well displayed, making it ideal for the assessment of the plant infection characteristics.

We measured the growth indices of poplar plants after transplanting for 70 days. As an important carrier of plant growth and development, the soil affects the plant quality. Different soils have different water and fertilizer retention capacities, resulting in differences in nutrient status, leading to differences in soil biological characteristics and crop root nutrient absorption and utilization [25]. We selected four types of culture media, and 1/2 MS was added to each medium to provide the necessary elements required by the plants. The combined culture media of vermiculite + 1/2 MS, sand + 1/2 MS, clay + 1/2 MS, and loam + 1/2 MS did not affect the leaf length and width, main root length, or the lateral roots of the poplar. Among the four combined soil materials, the imaging quality of the X-ray CT method was the highest under soil matrices of vermiculite and 1/2 MS. Soil background noise is an important factor affecting X-ray CT imaging. After acquiring images, the Avizo Fire (V 9. 0) software is used to remove the background noise. This method is simple and

effectively denoises the background to obtain a clear image, and the combined soil matrix does not affect the growth of poplar.

This study used X-ray CT to characterize the root decay of poplar infected by *A. solidipes*. X-ray CT imaging showed that the root of the control group had a regular epidermis from top to bottom, and that the internal density was uniform. However, in the experimental group, the root epidermis of poplar infected by *A. solidipes* appeared irregular from top to bottom, and changes in the internal density were uneven. It is shown that *A. solidipes* causes damage to the wood fibers in the poplar root, resulting in internal decay. Moreover, *A. solidipes* infection gradually spreads upward from the ground and inwards from the epidermis. Our findings elucidate on the infection processes of *A. solidipes* in poplar. The ARR of poplar often occurs in the early stages of growth, and it does not result in the expressions of any symptoms in the aerial parts of the poplar. Donnelly et al. [26] stated that symptoms of ARR appear when the infection is in advanced stages, and has no therapeutic value. Therefore, understanding the infestation process is crucial for disease control. X-ray CT is an effective method for observing the early roots of poplar. The pathogenic mechanism of ARR disease can be better understood by effectively quantifying the decayed site and area.

This study used the X-ray CT technique for the 3D reconstruction of poplar root images. The X-ray CT technique was used in this study because of its successful applications in the medical field [27]. Medical X-ray CT equipment has a fast scanning speed, high image resolution, and rich image post-processing functions [28,29]. Therefore, X-ray CT can be used to observe the configurations of the plant roots and to visualize the in situ morphologies of poplar roots. Findings from the manual measurements of the total root length, root bifurcation number, root apex number, and root mean diameter were consistent with the findings obtained by the software after 3D reconstruction. The results obtained after 3D reconstruction show that the root tip first develops the infection and symptoms. Then, the infection spreads upwards and gradually inwards, causing the epidermis, phloem, and xylem to decay. Verma [30] found that the destruction of wheat taproots by pathogenic bacteria significantly affected plant growth and reduced their ability to recover from the disease. Wheat makes up for this deficiency by producing more than one taproot, thereby minimizing the damage caused by pathogenic infection. This study did not find any lateral roots after the 3D reconstruction of poplar, indicating that after the infection of poplar by *A. solidipes*, the diseased roots lost the compensation phenomenon. Studies have shown that *Armillaria* produces secondary metabolites, aryl esters, which have the ability to inhibit plant cell growth [31,32]. We postulated that *A. solidipes* produces some metabolites that inhibit the compensatory abilities of poplar roots. It provides good material for studying the root etiology and configuration of forest trees.

5. Conclusions

X-ray CT is an accurate, rapid, and non-destructive in situ morphological observation and measurement technique for assessing plant root infections. We investigated the effects of four combinations of soil matrices on the X-ray CT imaging results of plant roots. The vermiculite + 1/2 MS combination was the best soil matrix for X-ray CT imaging, as it did not affect poplar growth. After 3D reconstruction of the control and experimental groups using the RadiAnt DICOM Viewer software, the root branches of the poplar were clear, and complete and manual measurements of total root length, total root volume, root forks, number of root tip, and root surface area were consistent with those measured using the Win-RHIZO 2017a software. After scanning the insides of the main root, it was found that the root tip first developed the infection. Then, the infection gradually spread upwards, from the epidermis to the phloem and xylem. In conclusion, the vermiculite + 1/2 MS combination is an optimal soil matrix that is suitable for X-ray CT imaging. It provides good material for studying the root etiology and configuration of forest trees.

Author Contributions: Formal analysis and funding acquisition, P.Z., G.X. and L.W.; investigation and methodology, M.K.; project administration, Y.X.; supervision, Y.X.; validation, L.W.; writing—original draft, P.Z.; writing—review and editing, Y.X. and L.W.; writing—editing, T.v.d.L. All authors have read and agreed to the published version of the manuscript.

Funding: This work was financed by the Special Project for Double First-Class—Cultivation of Innovative Talents (000/41113102) by Ping Zhang. Ping Zhang is grateful to the China Scholarship Council for the financial support (No. 202006600025).

Institutional Review Board Statement: Not applicable.

Informed Consent Statement: Not applicable.

Data Availability Statement: *A. solidipes* (A2001) strain internal transcribed spacer information was stored in NCBI GenBank, with the accession number OP787670.1.

Conflicts of Interest: The authors declare that they have no conflicts of interest.

References

- Rizzo, D.M.; Blanchette, R.A.; Palmer, M.A. Biosorption of metal-ions by *Armillaria*-rhizomorphs. *Can. J. Bot.* **1992**, *70*, 1515–1520. [[CrossRef](#)]
- Cromey, M.G.; Drakulic, J.; Beal, E.J.; Waghorn, I.; Perry, J.N.; Clover, G. Susceptibility of garden trees and shrubs to *Armillaria* root rot. *Plant. Dis.* **2020**, *104*, 483–492. [[CrossRef](#)] [[PubMed](#)]
- Klopfenstein, N.B.; Stewart, J.E.; Ota, Y.; Hanna, J.W.; Richardson, B.A.; Ross-Davis, A.L.; Elias-Roman, R.D.; Korhonen, K.; Keca, N.; Iturrutxa, E.; et al. Insights into the phylogeny of Northern Hemisphere *Armillaria*: Neighbor-net and Bayesian analyses of translation elongation factor 1-alpha gene sequences. *Mycologia* **2017**, *109*, 75–91. [[CrossRef](#)] [[PubMed](#)]
- Labbe, F.; Marcais, B.; Dupouey, J.L.; Belouard, T.; Capdevielle, X.; Piou, D.; Robin, C.; Dutech, C. Pre-existing forests as sources of pathogens? The emergence of *Armillaria ostoyae* in a recently planted pine forest. *For. Ecol. Manag.* **2015**, *357*, 248–258. [[CrossRef](#)]
- Cleary, M.R.; van der Kamp, B.J.; Morrison, D.J. Effects of wounding and fungal infection with *Armillaria ostoyae* in three conifer species. II. Host response to the pathogen. *Forest. Pathol.* **2012**, *42*, 109–123. [[CrossRef](#)]
- Coetzee, M.; Bloomer, P.; Wingfield, M.J.; Wingfield, B.D. Paleogene radiation of a plant pathogenic mushroom. *PLoS ONE* **2011**, *6*, e28545. [[CrossRef](#)]
- Warwell, M.V.; McDonald, G.I.; Hanna, J.W.; Kim, M.S.; Lalande, B.M.; Stewart, J.E.; Hudak, A.T.; Klopfenstein, N.B. *Armillaria altimontana* is associated with healthy western white pine (*Pinus monticola*): Potential in situ biological control of the *Armillaria* root disease pathogen, *A. solidipes*. *Forests* **2019**, *10*, 294. [[CrossRef](#)]
- Kranz, J.; Rotem, J. *Experimental Techniques in Plant Disease Epidemiology*; Springer: Berlin/Heidelberg, Germany, 1988. [[CrossRef](#)]
- Topp, C.N.; Bray, A.L.; Ellis, N.A.; Liu, Z.B. How can we harness quantitative genetic variation in crop root systems for agricultural improvement? *J. Integr. Plant. Biol.* **2016**, *58*, 213–225. [[CrossRef](#)]
- Han, L.; Dutilleul, P.; Prasher, S.O.; Beaulieu, C.; Smith, D.L. Assessment of common scab-inducing pathogen effects on potato underground organs via computed tomography scanning. *Phytopathology* **2008**, *98*, 1118–1125. [[CrossRef](#)]
- Han, L.; Dutilleul, P.; Prasher, S.O.; Beaulieu, C.; Smith, D.L. Assessment of density effects of the common scab-inducing pathogen on the seed and peripheral organs of potato during growth using computed tomography scanning data. *Trans. ASABE* **2009**, *52*, 305–311. [[CrossRef](#)]
- Peters, J.; Gauthey, A.; Lopez, R.; Carins-Murphy, M.R.; Brodribb, T.J.; Choat, B. Non-invasive imaging reveals convergence in root and stem vulnerability to cavitation across five tree species. *J. Exp. Bot.* **2020**, *71*, 6623–6637. [[CrossRef](#)] [[PubMed](#)]
- Chigwaya, K.; du Plessis, A.; Viljoen, D.W.; Crouch, I.J.; Crouch, E.M. Use of X-ray computed tomography and 3D image analysis to characterize internal browning in ‘Fuji’ apples after exposure to CO₂ stress. *Sci. Hortic.* **2021**, *277*, 109840. [[CrossRef](#)]
- Ma, T.M.; Gafita, A.; Shabsovich, D.; Juarez, J.; Grogan, T.R.; Thin, P.; Armstrong, W.; Sonni, I.; Nguyen, K.; Lok, V.; et al. Identifying the best candidates for prostate-specific membrane antigen positron emission tomography/computed tomography as the primary staging approach among men with high-risk prostate cancer and negative conventional imaging. *Eur. Urol. Oncol.* **2022**, *5*, 100–103. [[CrossRef](#)]
- Fedewa, S.A.; Kazerooni, E.A.; Studts, J.L.; Smith, R.A.; Bandi, P.; Sauer, A.G.; Cotter, M.; Sineshaw, H.M.; Jemal, A.; Silvestri, G.A. State variation in low-dose computed tomography scanning for lung cancer screening in the United States. *JNCI J. Natl. Cancer Inst.* **2021**, *113*, 1044–1052. [[CrossRef](#)]
- Atkinson, J.A.; Pound, M.P.; Bennett, M.J.; Wells, D.M. Uncovering the hidden half of plants using new advances in root phenotyping. *Curr. Opin. Biotech.* **2019**, *55*, 1–8. [[CrossRef](#)] [[PubMed](#)]
- Cochard, H.; Herbette, S.; Barigah, T.; Badel, E.; Ennajeh, M.; Vilagrosa, A. Does sample length influence the shape of xylem embolism vulnerability curves? A test with the cavitron spinning technique. *Plant Cell Environ.* **2010**, *33*, 1543–1552. [[CrossRef](#)] [[PubMed](#)]
- Moradi, A.B.; Conesa, H.M.; Robinson, B.; Lehmann, E.; Kuehne, G.; Kaestner, A.; Oswald, S.; Schulin, R. Neutron radiography as a tool for revealing root development in soil: Capabilities and limitations. *Plant Soil* **2009**, *318*, 243–255. [[CrossRef](#)]

19. Xu, Z.; Valdes, C.; Clarke, J. Existing and potential statistical and computational approaches for the analysis of 3D CT images of plant roots. *Agronomy* **2018**, *8*, 71. [[CrossRef](#)]
20. Wolfgang, B. *Methods of Studying Root Systems*; Springer: Berlin/Heidelberg, Germany, 1979. [[CrossRef](#)]
21. van der Weele, C.M.; Jiang, H.S.; Palaniappan, K.K.; Ivanov, V.B.; Palaniappan, K.; Baskin, T.I. A new algorithm for computational image analysis of deformable motion at high spatial and temporal resolution applied to root growth. Roughly uniform elongation in the meristem and also, after an abrupt acceleration, in the elongation zone. *Plant Physiol.* **2003**, *132*, 1138–1148. [[CrossRef](#)]
22. van Veelen, A.; Tourell, M.C.; Koebernick, N.; Pileio, G.; Roose, T. Correlative visualization of root mucilage degradation using X-ray CT and MRI. *Front. Environ. Sci.* **2018**, *6*, 32. [[CrossRef](#)]
23. Indore, N.S.; Karunakaran, C.; Jayas, D.S. Synchrotron tomography applications in agriculture and food sciences research: A review. *Plant Methods* **2022**, *18*, 1–26. [[CrossRef](#)]
24. Dhaliwal, J.K.; Kumar, S. 3D-visualization and quantification of soil porous structure using X-ray micro-tomography scanning under native pasture and crop-livestock systems. *Soil Tillage Res.* **2022**, *218*, 105305. [[CrossRef](#)]
25. Cardoso, D.; Martinez, H.; Pereira, A.M.; Kasuya, M.; Cecon, P.R. Potassium and growth-promoting fungi improve the postharvest quality of grape tomato. *Semin. Ciências Agrárias* **2022**, *43*, 675–692. [[CrossRef](#)]
26. Donnelly, D.; Sanada, S.; Oreilly, J.; Polonsky, J.; Prange, T.; Pascard, C. Isolation and structure (X-ray-analysis) of the Orsellinate of Armillol, a new antibacterial metabolite from *Armillaria-mellea*. *J. Chem. Soc. Chem. Commun.* **1982**, *2*, 135–137. [[CrossRef](#)]
27. Birnbacher, L.; Braig, E.M.; Pfeiffer, D.; Pfeiffer, F.; Herzen, J. Quantitative X-ray phase contrast computed tomography with grating interferometry biomedical applications of quantitative X-ray grating-based phase contrast computed tomography. *Eur. J. Nucl. Med. Mol. Imaging* **2021**, *48*, 4171–4188. [[CrossRef](#)]
28. Schmidt, B.; Flohr, T. Principles and applications of dual source CT. *Phys. Med.* **2020**, *79*, 36–46. [[CrossRef](#)]
29. Gong, H.; Ren, L.Q.; Hsieh, S.S.; McCollough, C.H.; Yu, L.F. Deep learning enabled ultra-fast-pitch acquisition in clinical X-ray computed tomography. *Med. Phys.* **2021**, *48*, 5712–5726. [[CrossRef](#)]
30. Verma, P.R. Biology and control of *Rhizoctonia solani* on rapeseed: A review. *Phytoprotection* **1996**, *77*, 99–111. [[CrossRef](#)]
31. Devkota, P.; Hammerschmidt, R. The infection process of *Armillaria mellea* and *Armillaria solidipes*. *Physiol. Mol. Plant Pathol.* **2020**, *112*, 101543. [[CrossRef](#)]
32. Baumgartner, K.; Coetzee, M.; Hoffmeister, D. Secrets of the subterranean pathosystem of *Armillaria*. *Mol. Plant Pathol.* **2011**, *12*, 515–534. [[CrossRef](#)]